

Setting Clock Speed in Mammals: The CK1 ϵ *tau* Mutation in Mice Accelerates Circadian Pacemakers by Selectively Destabilizing PERIOD Proteins

Qing-Jun Meng,^{1,6} Larisa Logunova,^{1,6} Elizabeth S. Maywood,^{2,6} Monica Gallego,³ Jake Lebiecki,¹ Timothy M. Brown,¹ Martin Sládek,² Andrei S. Semikhodskii,¹ Nicholas R.J. Glossop,¹ Hugh D. Piggins,¹ Johanna E. Chesham,² David A. Bechtold,¹ Seung-Hee Yoo,⁴ Joseph S. Takahashi,⁴ David M. Virshup,⁵ Raymond P. Boot-Handford,¹ Michael H. Hastings,^{2,*} and Andrew S.I. Loudon^{1,*}

¹Faculty of Life Sciences, University of Manchester, Stopford Building, Oxford Road, Manchester M13 9PT, UK

²MRC Laboratory of Molecular Biology, Neurobiology Division, Hills Road, Cambridge CB2 0QH, UK

³Department of Pediatrics, University of Utah, Salt Lake City, UT 84112, USA

⁴Howard Hughes Medical Institute, Department of Neurobiology & Physiology, Northwestern University,

2205 Tech Drive, Evanston, IL 60208-3520, USA

⁵Program in Cancer and Stem Cell Biology, Duke/NUS Graduate Medical School Singapore, 2 Jalan Bukit Merah 169547, Singapore

⁶These authors contributed equally to this work.

*Correspondence: andrew.loudon@manchester.ac.uk (A.S.I.L.), mha@mrc-lmb.cam.ac.uk (M.H.H.)

DOI 10.1016/j.neuron.2008.01.019

SUMMARY

The intrinsic period of circadian clocks is their defining adaptive property. To identify the biochemical mechanisms whereby casein kinase 1 (CK1) determines circadian period in mammals, we created mouse null and *tau* mutants of *Ck1 epsilon*. Circadian period lengthened in CK1 $\epsilon^{-/-}$, whereas CK1 $\epsilon^{tau/tau}$ shortened circadian period of behavior in vivo and suprachiasmatic nucleus firing rates in vitro, by accelerating PERIOD-dependent molecular feedback loops. CK1 $\epsilon^{tau/tau}$ also accelerated molecular oscillations in peripheral tissues, revealing its global role in circadian pacemaking. CK1 ϵ^{tau} acted by promoting degradation of both nuclear and cytoplasmic PERIOD, but not CRYPTOCHROME, proteins. Together, these whole-animal and biochemical studies explain how *tau*, as a gain-of-function mutation, acts at a specific circadian phase to promote degradation of PERIOD proteins and thereby accelerate the mammalian clockwork in brain and periphery.

INTRODUCTION

In mammals, daily rhythms of sleep and metabolism are driven by the circadian pacemaker within the suprachiasmatic nuclei of the hypothalamus (SCN) which coordinates the activity of subordinate circadian clocks in other brain regions and in peripheral tissues (Reppert and Weaver, 2002; Hastings et al., 2003; Lowrey and Takahashi, 2004; Saper et al., 2005). Precise maintenance of circadian period is the defining adaptive property of these clocks. In both brain and periphery, a central concept is that circadian clocks consist of interlocked autoregulatory feedback loops in which CLOCK:BMAL1 heterodimers bind to E box

DNA sequences contained within genes encoding the transcriptional repressors PER and CRY. Following their accumulation in the cytoplasm, PER:CRY complexes translocate to the nucleus after a delay of several hours and repress the activity of constitutively bound CLOCK:BMAL1 complexes. These inhibitory complexes are then degraded following a further delay, and the derepression of CLOCK:BMAL1 activity initiates the next circadian cycle of *Per* and *Cry* transcription. Mutations in various elements of this core molecular clock have been described, many of which result in either arrhythmia or alteration in period of rest/activity and sleep cycles.

In addition to periodic transcription, posttranslational modifications of clock proteins are crucial for the correct operation of molecular clockworks (Lee et al., 2001; Gallego and Virshup, 2007). In particular, reversible phosphorylation provides a potential mechanism for the regulated formation of protein complexes, their nuclear entry, and ultimate degradation via ubiquitination pathways, each step of which introduces delays into the feedback loop. Current interest has focused on the role that protein phosphorylation may play in tuning the circadian oscillator to a period of 24 hr. In *Drosophila*, mutations of CK1 (*doubletime*, DBT) were the first circadian mutants discovered to involve an enzyme and resulted in either short (*dbt^s*) or long (*dbt^l*) rhythms of eclosion and locomotor activity (Kloss et al., 1998; Price et al., 1998).

The *tau* mutation of Syrian hamsters was the first mammalian circadian mutation discovered. It causes significant shortening of activity cycles to 20 hr and assorts in a Mendelian fashion (Ralph and Menaker, 1988). Subsequent mapping studies revealed that this mutation resided within casein kinase 1 ϵ as a C to T transversion in position 178 (Lowrey et al., 2000). Protein expression studies suggested a destabilization of nuclear PER in the *tau* mutant hamster (Dey et al., 2005), while recent modeling and biochemical studies suggested that *tau* is a gain-of-function mutation on specific residues within the PER protein target (Gallego and Virshup, 2007), likely leading to increased degradation, altered stability, and accelerated protein turnover. It is unknown

whether these latter conclusions, developed in cultured cells and mathematical modeling studies, reflect the real circumstances in living animals. Further, it is unclear whether altered degradation of PER involves cellular compartmentalization, whether it is tissue specific (neural versus peripheral), and ultimately how it leads to accelerated molecular timing in the SCN.

To define the role of CK1 ϵ in the circadian clockwork, and hence the molecular disturbance underlying advanced sleep phase disorder and accelerated circadian period, we describe here the generation of a mouse model of the hamster *tau* mutation within CK1 ϵ . We adapted the *loxP-cre* strategy to produce mice carrying the *tau* allele of the *Ck1 ϵ* gene and used subsequent *cre*-mediated in vivo disruption of exon 4, which encodes the catalytic domain of CK1 ϵ (Lowrey et al., 2000) to generate a *Ck1 ϵ* null allele. This allelic series was assayed by circadian behavioral wheel-running and SCN electrophysiological studies and revealed that *tau* acts as a gain-of-function mutation, shortening period in a dose-dependent manner. By using PER2 protein reporters (Yoo et al., 2004), we also define, for the first time, the impact of this mutation on the molecular dynamics of both the SCN and peripheral timers and, within the SCN, highlight the role of accelerated protein turnover in shortening circadian period and activity/rest cycles. Finally, western blotting and imaging studies of both transfected cell lines, primary fibroblasts and SCN tissue derived from CK1 ϵ ^{*tau*} mice reveal that CK1 ϵ ^{*tau*} specifically targets PERIOD but not CRY proteins during the early nocturnal phase of the circadian cycle, acting on one component of the negative feedback element of the clock, and leading to an acceleration of period by an asymmetric degradation of PER proteins at a specific phase of the circadian cycle.

RESULTS AND DISCUSSION

Generation of a *tau* Mutant Allele for CK1 ϵ and Subsequent Disruption

We adapted the *loxP-cre* recombinase strategy used for creating a conditional knockout to produce a mouse carrying the *tau* allele of the *Ck1 ϵ* gene. This can be subsequently converted in vivo to a *Ck1 ϵ* gene knockout by *cre*-mediated ablation of exon 4, which encodes the catalytic domain of CK1 ϵ (Lowrey et al., 2000; see Figure S1A available online). Deletion of exon 4 leads to a frameshift and premature stop codon. The linearized targeting vector was electroporated into ES cells and G418 resistant, homologously recombined ES clones (Figure S1B) subjected to transient transfection with *cre* recombinase followed by FIAU selection. Resistant colonies that had deleted the selection cassette but retained the mutant *tau* exon were identified by PCR (Figure S1C) and used to generate germline transmitting chimeras. The presence of the *tau* mutation (the C to T transversion at amino acid position 178) in the founder transgenic mice was confirmed by sequencing of animal-derived genomic DNA through the *tau* site (Figure S1D). F1 mice carrying the floxed *tau* allele were crossed with a deleterious *cre* mouse to generate the *Ck1 ϵ* knockout line. Gene knockout was confirmed genetically by genomic DNA sequencing of the *Ck1 ϵ* gene as well as by RT-PCR using brain cDNA as templates (Figure S1E). The absence of the CK1 ϵ protein was also confirmed by western blotting in whole-brain extracts using an antibody against the C terminus of CK1 ϵ (Figure S1F). Mice carrying the

tau allele (*tau*/+ and *tau*/*tau*) or the knockout allele (−/+ and −/−) were viable and fertile with no overt deleterious phenotype.

The *tau* Mutation Shortens and the Null Mutation of CK1 ϵ Lengthens Period

All wild-type and knockout mice entrained to LD 12 hrL:12 hrD exhibited activity in the dark phase, commencing shortly after lights off. In contrast, *tau* mice exhibited variable responses to LD 12L:12D cycles, and in a sample of 30 animals, 9 exhibited a phase advance of the LD cycle, 5 exhibited masking with onsets coincident with dark onset, and 16 animals free-ran across the prevailing LD cycle (Figures S2A–S2C). To determine the impact of CK1 ϵ ^{*tau*} on free-running behavior, we monitored wheel-running activity in constant darkness (DD). CK1 ϵ ^{*tau*} mice exhibited significant shortening of period in a dose-dependent manner (Figures 1A and 1B): 23.6 ± 0.05 hr for wild-type (WT), 21.8 ± 0.08 hr for heterozygote (CK1 ϵ ^{*tau*/+}), and 20.0 ± 0.07 hr for homozygotes (CK1 ϵ ^{*tau*/*tau*}). This is equivalent to 1.80 hr/copy of CK1 ϵ ^{*tau*} and virtually identical to the behavioral phenotype of this mutation in Syrian hamsters (6). In contrast, knockout mice exhibited a small but significant period lengthening compared to their WT counterparts (24.0 ± 0.06 versus 23.6 ± 0.05 hr, respectively, *p* < 0.001; Figures 1A and 1B). Importantly, mice carrying a single copy of the knockout allele exhibited a WT-like free-running period of 23.7 ± 0.05 hr, while the *tau* hemizygote (CK1 ϵ ^{*tau*/−}, 21.6 ± 0.09 hr) and heterozygote (CK1 ϵ ^{*tau*/+}) mice exhibited virtually identical periods (Figures 1A and 1B). This shows that a single WT copy of *Ck1 ϵ* provides little protective effect in the face of a *tau* allele and thus offers definitive genetic evidence that *tau* acts as a gain-of-function mutation.

Interestingly, the absolute number of wheel revolutions per circadian cycle was similar in all genotypes, suggesting period acceleration in the *tau* mutants may occur due to an asymmetric effect on overall circadian organization, perhaps sparing nocturnal activity per se (Figures 1C and 1D). Similar effects are reported for circadian mutations in DBT (Price et al., 1998), the CK1 ortholog in *Drosophila*. The asymmetric acceleration of circadian timing was extended in studies of metabolic rhythms in the CK1 ϵ ^{*tau*} and WT mice using indirect calorimetry. Here, we noted that there was a compression of circadian rhythms of oxygen consumption (VO₂) in CK1 ϵ ^{*tau*} mice which closely matched the periods determined earlier by wheel running (Figure 2). Remarkably, the pattern of oxygen consumption was highly asymmetric such that the shortening of period was almost entirely associated with a compression of the inactive (subjective day) phase (active phase duration, WT = 12.6 ± 0.1 hr; CK1 ϵ ^{*tau*} = 13.4 ± 0.6 hr; inactive phase duration, WT = 11.4 ± 0.1 hr; CK1 ϵ ^{*tau*} = 6.9 ± 0.5 hr; *p* < 0.01; Figures 2B and 2C). Hence, our data suggest that the absolute duration of nocturnal physiology and behavior were unaffected by the CK1 ϵ ^{*tau*} mutation, rather, nocturnal events were initiated earlier in CK1 ϵ ^{*tau*} than in WT. Such observations are compatible with our earlier demonstration in *tau* mutant hamsters of an advanced onset of circadian nocturnal melatonin secretion, with the result that overall duration of secretion of this nocturnal hormone is identical to that of wild-types (Lucas et al., 1999). Collectively, these data suggest that CK1 ϵ ^{*tau*} may accelerate period by compressing a specific phase of the circadian behavioral and physiological

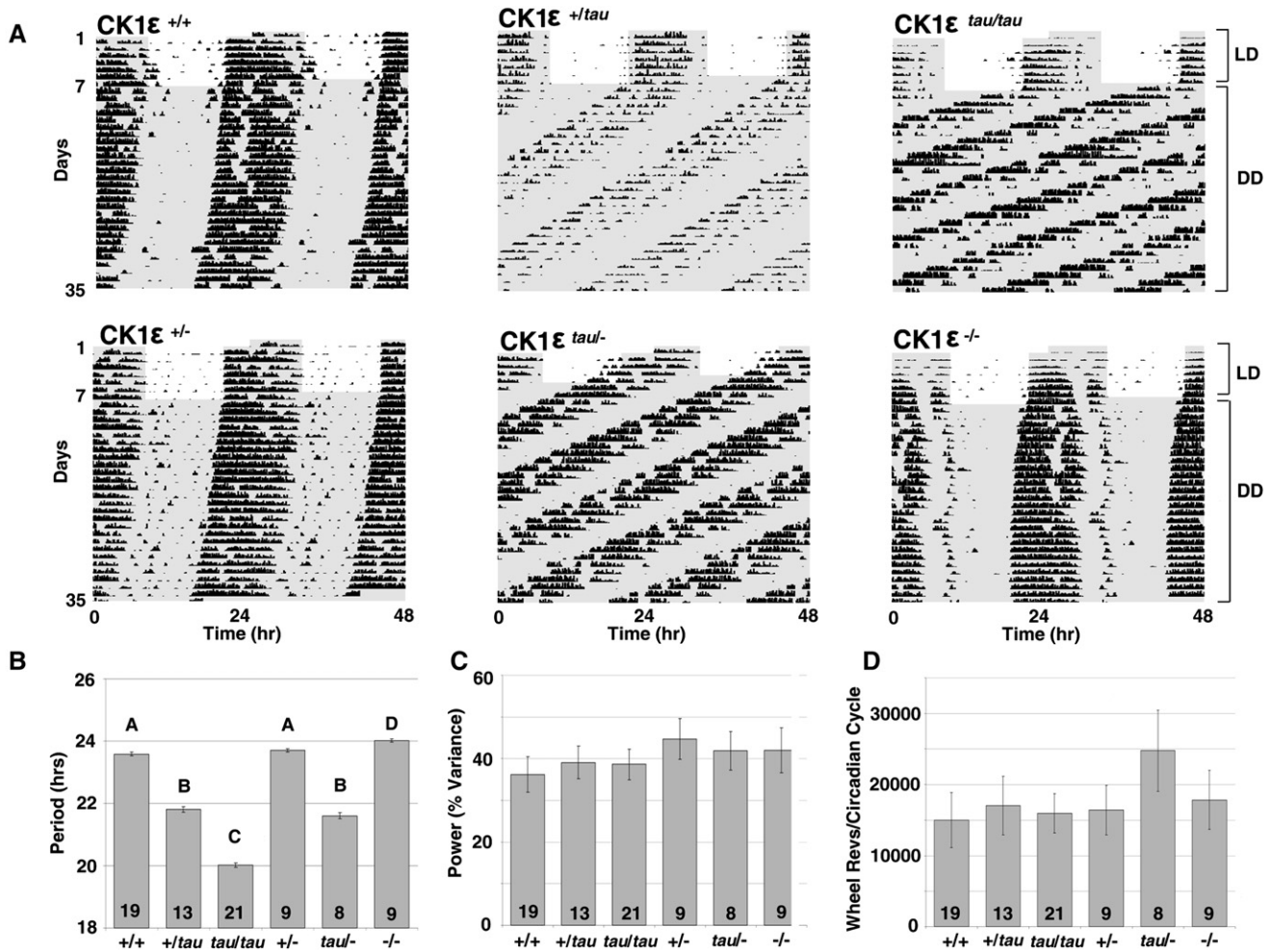


Figure 1. Locomotor Activity Rhythms for Wild-Type, *tau* Mutant, and Knockout Mice

(A) Representative wheel-running activity records (actograms) for wild-type ($CK1\epsilon^{+/+}$; top-left panel), heterozygous ($CK1\epsilon^{+tau}$; top-middle panel), homozygous ($CK1\epsilon^{tau/tau}$; top-right panel), hemizygous ($CK1\epsilon^{+/-}$; bottom-left panel), hemizygous tau ($CK1\epsilon^{tau/-}$; bottom-middle panel), and $CK1\epsilon$ knockout mice ($CK1\epsilon^{-/-}$; bottom-right panel) are shown in double-plotted format. Each horizontal line represents 48 hr, with the second day plotted to the right and one cycle below the first cycle. Animals were run in 24 hr cycles of 12 hr Light, 12 hr Dark (LD) and then in continuous darkness (DD). The timing of the LD cycles is indicated by the alternating white and gray areas of the actogram.

(B) Periodogram estimates of period for each genotype as mean \pm SEM; the number of animals is indicated within each bar. Bars with different letters show a significant difference ($p < 0.001$ ANOVA and post-hoc Bonferroni compared to wild-type); bars with the same letter are not significantly different.

(C) Circadian amplitude (power from periodogram analyses) for each genotype. There was no significant difference between genotypes (mean \pm SEM).

(D) Activity levels during the first 4 weeks of DD for each genotype as determined by total wheel-running revolutions per circadian cycle. There were no significant differences between genotypes despite shortened overall circadian period (mean \pm SEM).

cycle. In the case of the knockout mice, the circadian phenotype was mild (ca 18 min extension in period). Although we have not undertaken measures of oxygen consumption in knockout mice, our analysis of the relative proportion of the circadian cycle in which knockout animals are active (alpha) and the overall structure of the circadian activity cycle revealed that they were not significantly different to wild-types.

Individual Neurons of the SCN Exhibit an Accelerated Firing Rate in $CK1\epsilon^{tau}$ Mutants

In order to extend our studies to the SCN, we adopted the use of a suction electrode method which permits discrimination of firing

rate profiles for individual cells for over 48 hr in vitro (Brown et al., 2006). Using acutely prepared SCN slices, we recorded extracellular multiunit electrical activity in animals in which circadian periods had previously been recorded in running wheels in DD, permitting comparison of individual behavioral periods to SCN cellular rhythms. In all genotypes ($CK1\epsilon^{+/+}$, $CK1\epsilon^{tau/+}$, $CK1\epsilon^{tau/tau}$, $CK1\epsilon^{-/-}$), there was a close concordance with their period of multiunit recording in each slice (Figure 3A). SCN single-unit recordings revealed a similar outcome (Figure 3A), with a highly significant correlation ($r^2 = 0.83$, $p < 0.01$) between rhythms of single unit firing rates and behavior across all four genotypes (Figure 3B), indicating that effects of $CK1\epsilon^{tau}$ on behavioral

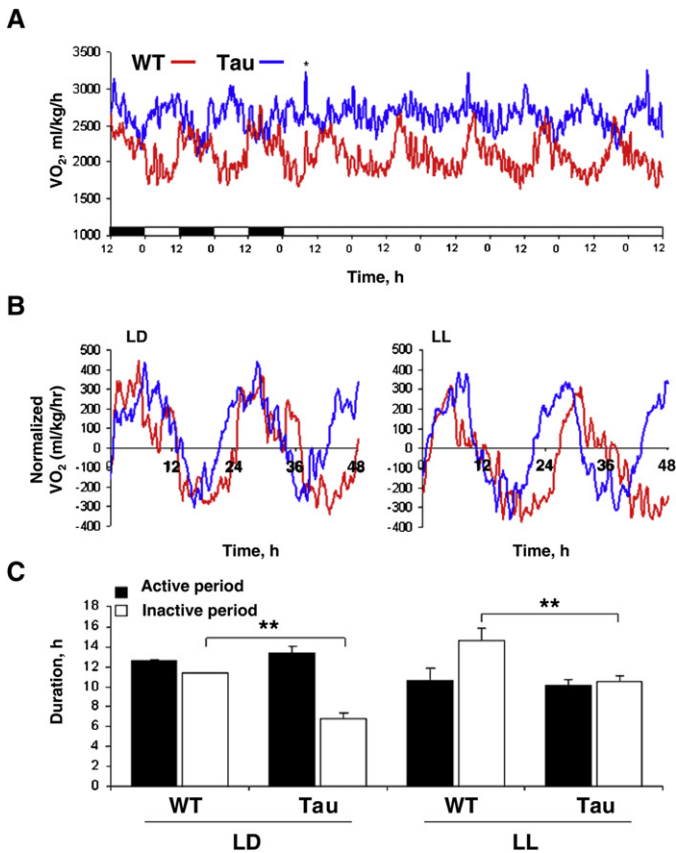


Figure 2. CK1 ϵ^{tau} Causes Asymmetric Acceleration of Circadian Timing in Metabolic Rhythms

(A) Representative recordings of oxygen consumption rhythms (VO₂) in WT (red) and *Tau* mutant (blue) mice across a segment of the light-dark (LD) and constant light (LL) cycles, showing an accelerated period in *Tau* mice. * indicates cages cleaned.

(B) Representative profiles of VO₂ for *Tau* and WT normalized to the midpoint (50%) of the trough-to-peak and peak-to-trough amplitudes. Rhythms are double plotted over a 48 hr time base. The “active” and “inactive” portions of the cycle were defined as the portions of the cycle above or below zero (respectively).

(C) Duration of the active (black) and inactive (open) phases of the circadian cycle (mean \pm SEM). Duration of active phase was maintained in *Tau* mice in both LD and LL, when compared with WT mice. In contrast, the inactive (subjective day) portion of the cycle was reduced in *Tau* mice under both light conditions. As expected, both genotypes exhibited a lengthening of the inactive period when switched from LD to LL. (** $p < 0.01$ post-hoc Bonferroni).

period likely arose from corresponding changes in circadian patterns of electrical activity of SCN neurons (Brown et al., 2005). The pattern of electrical activity of the knockout was normal in terms of amplitude and firing frequency, indicating that gene loss did not alter fundamental aspects of SCN electrophysiological properties. Thus, our generation of CK1 ϵ^{tau} in mice and subsequent gene deletion has resulted in a novel allelic series of circadian period, ranging from 20.0 (CK1 $\epsilon^{\text{tau/tau}}$) to 24.0 hr (CK1 $\epsilon^{-/-}$), and provides an unprecedented resource to explore the central role of CK1 to circadian rhythm regulation in mammals.

Impact of CK1 $\epsilon^{\text{tau/tau}}$ on the Molecular Pacemaker of the SCN and Peripheral Tissues

Accelerated circadian periods of activity/rest cycles and also SCN firing rates likely reflect altered dynamics within molecular feedback loops that underpin circadian time-keeping within the SCN. To determine the impact of CK1 ϵ on SCN molecular oscillators, CK1 ϵ^{tau} mice were crossed into PER2::Luciferase (PER2::LUC) protein fusion reporter mice (Yoo et al., 2004). Organotypic SCN slices were prepared from 5- to 10-day-old pups and luciferase activity recorded using photomultiplier tubes (PMTs) over a minimum of 7–10 cycles. Bioluminescence recorded from PER2::LUC SCN slices closely matched behavioral rhythms for each genotype (Figures 4A and 4B): 24.4 \pm 0.15 hr, 21.9 \pm 0.08 hr, and 20.2 \pm 0.17 hr in CK1 $\epsilon^{+/+}$, CK1 $\epsilon^{\text{tau/+}}$, CK1 $\epsilon^{\text{tau/tau}}$ slices, respectively (ANOVA, $F = 226.5$, $p < 0.01$). To extend these studies to the single-cell level, we recorded PER2 expression of individual SCN neurons

measured using a CCD camera. Single-neuron imaging showed that circadian period of single neurons also matched genotype (24.9 \pm 0.09, 22.1 \pm 0.04, and 20.5 \pm 0.05 hr for CK1 $\epsilon^{+/+}$, CK1 $\epsilon^{\text{tau/+}}$, CK1 $\epsilon^{\text{tau/tau}}$, respectively) and that CK1 ϵ^{tau} had no effect on the intercellular synchrony nor regional distribution of circadian gene expression across the SCN (Figure 4C). Therefore, these bioluminescence recordings reveal that both the behavioral and electrophysiological impact of the CK1 ϵ^{tau} mutation is underpinned by accelerated molecular time-keeping within individual SCN neurons.

It is unknown whether endogenous CK1 ϵ has a global role in setting clock speed in tissues outside the nervous system. We therefore recorded circadian PER2::LUC activity in organotypic slices of pituitary, lung, and kidney and primary lung fibroblast cultures. This revealed clear circadian expression of PER2 and, on a group basis, a significant shortening of period by CK1 ϵ^{tau} (Figures S3A, 4B, and 4D). In contrast to the SCN, however, the magnitude of effect was variable across tissues, indicating partial penetrance of the mutation. Moreover, in lung and kidney, the *tau* allele significantly accelerated the rate of damping of the molecular cycle (Figure S3B). Thus, our *in vitro* data show that CK1 ϵ^{tau} accelerates pacemaking globally, although its detailed impact on SCN and peripheral oscillators is tissue specific.

We hypothesized from our *tau* mutant hamster studies that CK1 ϵ^{tau} may shorten period by accelerating the loss of nuclear PER proteins specifically in the early nocturnal phase (Dey et al., 2005), leading to earlier derepression of BMAL1 and CLOCK and overall circadian acceleration. This “asymmetric acceleration” model of PER protein turnover in CK1 ϵ^{tau} mutants was tested in our bioluminescence recordings of SCN slices. By aligning SCN waveforms from WT and CK1 ϵ^{tau} (Figure 4E) by either peak or nadir of expression, it is evident that the mutation significantly accelerates the decline of PER2::LUC (time to fall to 50% level WT = 5.3 \pm 0.3 hr, CK1 $\epsilon^{\text{tau/tau}}$ = 3.9 \pm 0.2 hr, ANOVA $F = 8.97$, $p < 0.01$). Consequently, the cycle in CK1 ϵ^{tau} homozygote slices is advanced by ca 3.4 hr compared to WT over the interval of PER protein decline (hours from peak to trough), whereas over the rising phase CK1 $\epsilon^{\text{tau/tau}}$ has little effect.

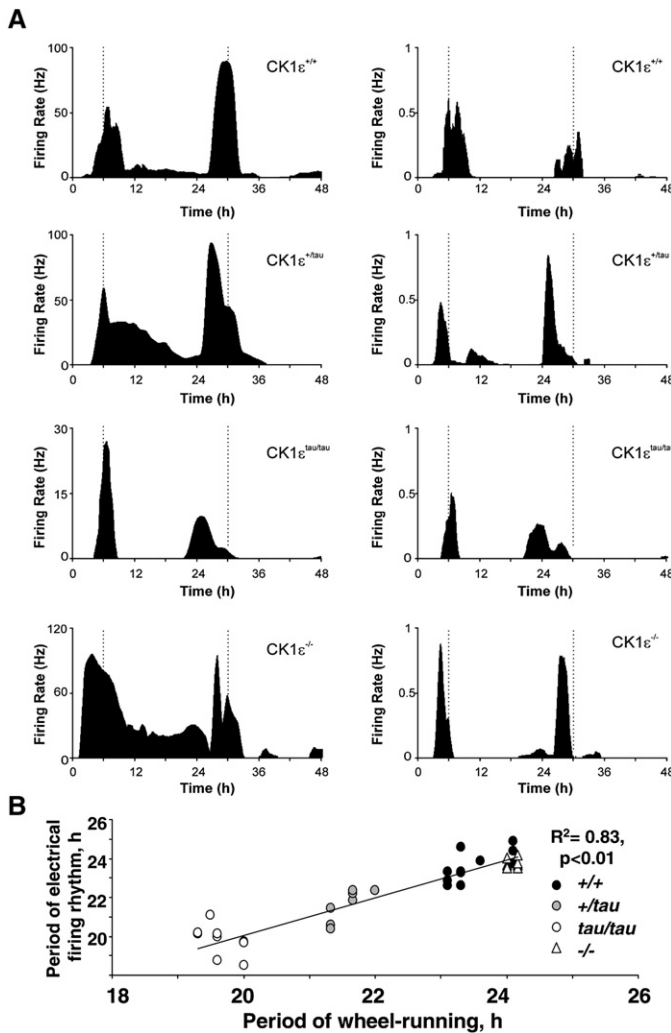


Figure 3. CK1 ϵ Mutations Alter Period of SCN Electrical Firing Rhythm

(A) Representative SCN multiunit (LH) and single-unit (RH) action potential discharge rhythms recorded from wild-type (CK1 ϵ ^{+/+}), heterozygote (CK1 ϵ ^{+/tau}), homozygote (CK1 ϵ ^{tau/tau}) and knockout mutant (CK1 ϵ ^{-/-}) brain slices.

(B) Correlation between period of wheel-running behavior determined in DD before slice preparation and subsequent single-unit SCN firing rates for WT (closed circles), *tau* heterozygote (gray circles) and homozygote (open circles), and null animals (triangles). Data are derived from 11 out of 13 CK1 ϵ ^{+/+} SCN neurons, 8/9 CK1 ϵ ^{+/tau}, 11/12 CK1 ϵ ^{tau/tau}, and 9/10 CK1 ϵ ^{-/-} cells that exhibited detectable firing-rate rhythms.

Additional statistical confirmation of this distorted waveform came from analysis of skewness (Figure S3C), slices with shorter periods having a more negative skew due to asymmetric distortion of waveform. Our data show that most of the accelerated degradation of PER within the SCN occurs at a specific phase and that this acceleration is consistent with, and can account for, the period changes observed in wheel-running behavior.

CK1 ϵ ^{tau} Selectively Accelerates PER Degradation Independently of Subcellular Localization

These data indicate that CK1 ϵ ^{tau} accelerates the onset of nocturnal processes (but not affecting their absolute duration) by accelerating the clearance of endogenous SCN PER2 proteins predominantly in the early circadian night. To explore the biochemical basis of this effect, we used real-time fluorescence videomicroscopy to monitor PER2::YFP degradation in COS-7 cells following blockade of de novo protein synthesis by treatment with cycloheximide (CHX, 20 μ g/ml). Coexpression with WT but not kinase-dead CK1 ϵ accelerated PER2::YFP protein degradation, relative to vector control. Degradation was further accelerated by CK1 ϵ ^{tau} (Figure 5A). In contrast, CRY1::CFP degra-

ation was not affected by any variants of CK1 ϵ , indicating a selective action of CK1 ϵ on PER2 (Figure 5B). Inhibition of nuclear export by leptomycin B (LMB) retained PER2::YFP in the nucleus and slowed its degradation in the presence of WT CK1 ϵ . In contrast, LMB did not alter the acceleration of PER2 degradation by CK1 ϵ ^{tau} (Figure 5C and 5D), confirming a nuclear site of action of this mutation. LMB could alter degradation rates by blocking PER nuclear export or by altering trafficking of other components required for PER degradation. To differentiate between these possibilities, to extend the range of cell types investigated, and to determine the effect of CK1 ϵ ^{tau} on PER1, we expressed in NIH 3T3 cells WT or mutant forms of PER1 in which either the nuclear export signal was mutated (mtNES) or an additional copy of the nuclear localization signal was added (+NLS). Both mutations trapped most of the PER1 within the nuclear compartment (>65% for mtNES; > 88% for +NLS) as determined by immunocytochemistry (Figure 5E). CK1 ϵ ^{tau} accelerated degradation, not only of wtPER1 as previously reported (Gallego et al., 2006) but also of nuclear-trapped PER1 (residual PER1 at 4 hr post-CHX treatment, CK1 ϵ ^{tau} versus WT, 45% and 81% for mtNES; 39% and 66% for +NLS; Figure 5F). In addition, CK1 ϵ ^{tau} accelerated degradation of another mutant form of PER1 (PER1₁₋₈₂₃) which lacked the C terminus that contains an active NLS as well as the CRY binding site (Vielhaber et al., 2001) and retained PER1 predominantly in the cytoplasm (>87%; Figures 5E and 5F). Together, these in vitro data clearly show that CK1 ϵ ^{tau} targets both PER1 and PER2 but not CRY1 proteins, and this selective targeting occurs regardless of nuclear or cytoplasmic localization.

CK1 ϵ ^{tau} Also Selectively Accelerates Endogenous PER Degradation in Primary Cells and SCN Slices

We extended these studies of recombinant protein stability by using western blots to examine native PER1 and CRY1 expression in WT and mutant primary fibroblast cultures. PER1 proteins typically exhibit two clear bands which represent hypo- (lower band) and hyperphosphorylated (upper band) forms of PER1 (Lee et al., 2001; Figure 6A). In *tau* mutant fibroblasts, the overall levels of PER1 were lower than those seen in WT cells. However, upon treatment with CHX (20 μ g/ml), the hyperphosphorylated forms of PER1 displayed a significantly shorter half-life in *tau* mutant cells than in WT cells (WT, 9.4 hr, versus *tau*, 4.0 hr, $p < 0.05$ using nonlinear exponential decay analysis with GraphPad;

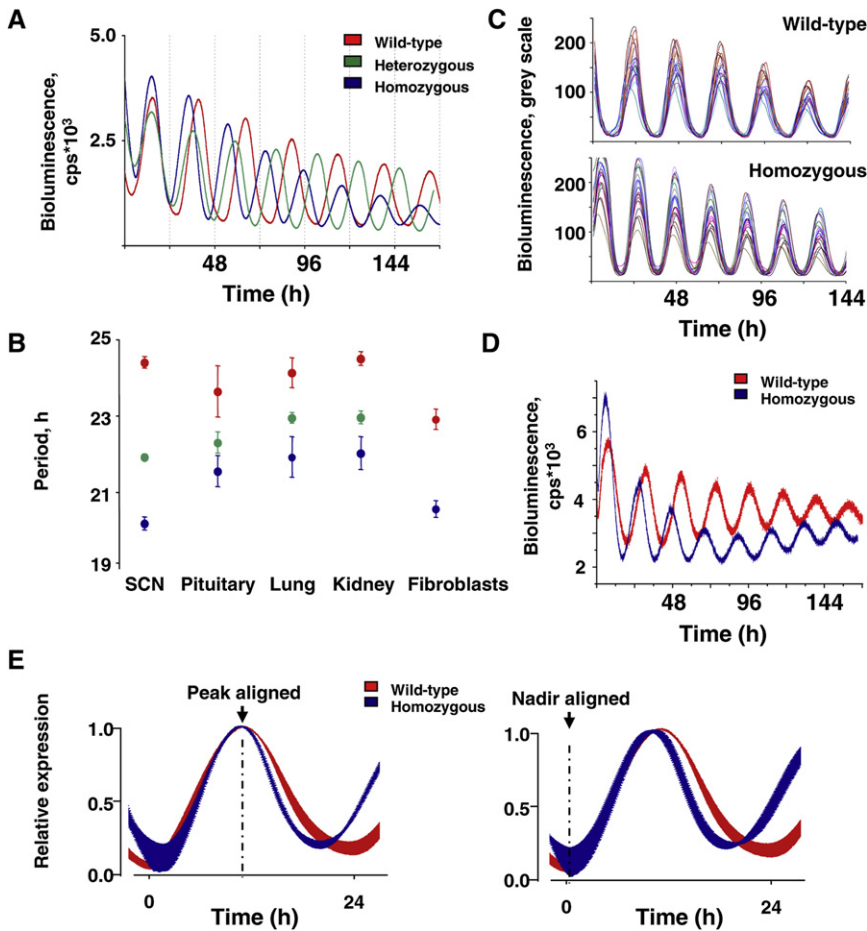


Figure 4. CK1 ϵ^{tau} Has a Global Impact on Circadian Pacemaking, Accelerating Molecular Circadian Oscillators in SCN, Peripheral Tissues, and Primary Fibroblasts

(A) Representative PER2::LUC bioluminescence oscillations in WT (red), heterozygote (green), and homozygote (blue) organotypic SCN slices. (B) The periodicity of tissues from WT, heterozygote, and homozygote *tau* PER2::LUC mice (mean \pm SEM; WT, $n = 4-6$; heterozygotes, $n = 10-11$; homozygote, $n = 5-6$).

(C) CCD recordings of SCN PER2::LUC expression at the single cell level for WT and homozygote SCN slices (20 per slice; $n = 3$ slices for each genotype). (D) Representative traces of PER2::LUC expression in primary fibroblast cultures of WT (red) and *tau* mutant (blue) mice.

(E) Waveform alignments by nadir or peak for PER2::LUC rhythms from WT (red) and homozygote (blue) organotypic SCN slices. Data were normalized and then plotted as mean \pm SEM ($n = 6$ per genotype). Note selective reduction in peak to nadir interval regardless of alignment.

Conclusions

In mammals, different forms of CK1 (CK1 ϵ and CK1 δ), act on diverse pathways, including Wnt signaling, neurotransmitter regulation, as well as circadian rhythms. Both CK1 ϵ and CK1 δ complex with PER and CRY (Lee et al., 2001), while CK1-mediated phosphorylation of BMAL1 increases its transcriptional activity (Eide et al., 2002). In humans, circadian familial advanced sleep disorders (FASPS) are known to be caused by a serine to glycine substitution in the *hPer2* gene at position 662 (Toh et al., 2001) and also by a T44A missense mutation in human *Ck1 δ* , which causes hypophosphorylation of PER2 (Xu et al., 2005). Transgenic mice overexpressing the *hPER2* mutation exhibit shorter free-running periods, mimicking FASPS (Xu et al., 2007), and their phenotype is sensitive to CK1 δ : increased dosage of CK1 δ shortens their period further. These studies, together with recent *in vitro* analyses of the equivalent serine residue on mouse PER2 protein (Vanselow et al., 2006) suggest that expression, degradation, nuclear entry and export of PER2 are modulated by multiple states of phosphorylation and that CK1 activity plays a central role at these various checkpoints of the circadian cycle (Gallego and Virshup, 2007; Mignot and Takahashi, 2007).

By creating null and *tau* mutations of CK1 ϵ in mice, we provide behavioral, neurophysiological, and cellular evidence showing that CK1 ϵ^{tau} acts as a gain of function that accelerates the molecular dynamics of circadian time-keeping. These biochemical actions explain the behavioral and physiological phenotype of the mutation in both hamsters and mice. They also provide a new perspective with which to understand the action of PER2 and CK1 mutations which have been linked to circadian period and sleep disturbances in humans (Xu et al., 2005, 2007). Our data therefore confirm and extend the earlier

(Figure 6B). This is consistent with the idea that hyperphosphorylated PER1 may be preferentially targeted to the proteasome for degradation (Gallego and Virshup, 2007). In contrast, the overall expression level and CHX-stimulated decline of CRY1 was unaffected by CK1 ϵ^{tau} (Figures 6A and 6B). To obtain a more dynamic view of PER degradation, we then exploited real-time recording of primary fibroblasts treated with CHX at the peak of PER2::LUC expression. This revealed that CK1 ϵ^{tau} significantly shortened ($p < 0.01$) the half-life of PER2::LUC expression, by ca. 25 min. Moreover, even though pretreatment with LMB extended the half-life in both genotypes, CK1 ϵ^{tau} was still effective at accelerating PER2::LUC degradation ($p < 0.01$; Figures 6C and 6D), consistent with the recombinant protein studies of a nuclear action for the mutation. Finally, we tested PER2::LUC degradation in the physiologically relevant context of the SCN slice, again adding CHX at the peak of circadian expression. As with the fibroblasts, loss of PER2::LUC bioluminescence was more rapid in mutant than WT SCN slices (Figures 6E and 6F), half-life again being shortened by ca. 25 min. Moreover, the effect of CK1 ϵ^{tau} remained following pretreatment with LMB, which had no significant effect on PER2::LUC clearance in either genotype. Together, these data demonstrate that CK1 ϵ^{tau} facilitates the degradation of endogenous PER (but not CRY) proteins in SCN and primary cells, and that blockade of nuclear export does not attenuate the *tau* phenotype.

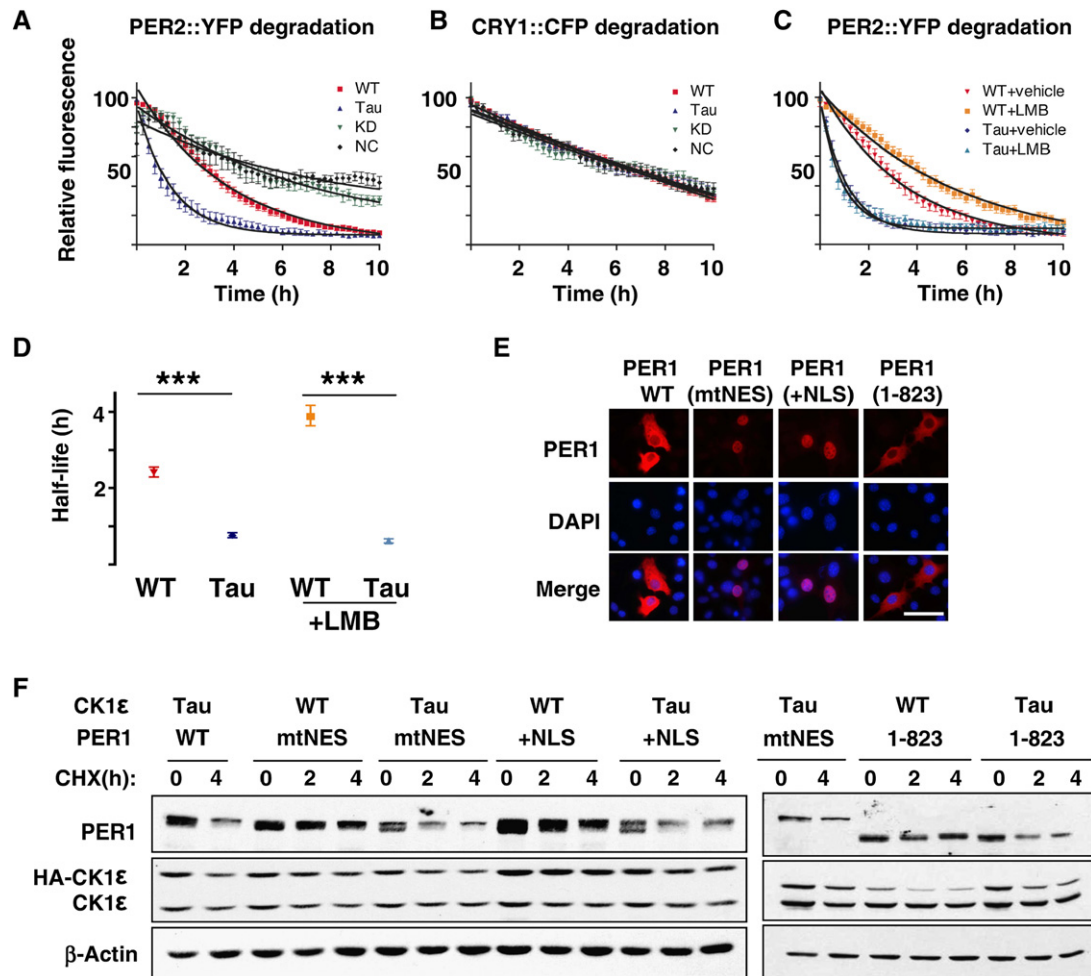


Figure 5. The *tau* Mutation Selectively Targets PER Proteins for Accelerated Degradation Independently of Their Cellular Localization

(A and B) Decay of PER2::YFP or CRY1::CFP fluorescence in COS-7 cells cotransfected with WT (red), *tau* (Tau, blue), kinase-dead (KD, green) CK1ε or empty plasmid (NC, black). Cells were treated with CHX (20 μg/ml) 0.5 hr before recording.

(C) Decay of PER2::YFP fluorescence in COS-7 cells treated with vehicle or leptomycin B (LMB, 10 ng/ml) 1 hr before CHX (20 μg/ml) (red, CK1ε WT + vehicle; yellow, WT + LMB; blue, *tau* mutant + vehicle; green, *tau* mutant + LMB). [(A–C) individual cell data normalized to maximum and minimum intensity over recording, plotted as mean ± SEM, n = 14–33, 2–4 independent experiments].

(D) Half-lives for PER2::YFP in presence of WT or *tau* CK1ε, treated with vehicle or LMB (mean ± 95% confidence limits, ***p < 0.001).

(E) Differential nuclear or cytoplasmic retention of Myc-tagged WT and mutant PER1 in NIH 3T3 cells. Scale bar = 500 μm.

(F) Western blots of Myc-tagged wild-type mPER1 or with mutated NES (mtNES), with extra NLS (+NLS) or truncated C terminus removing native NLS (1–823), coexpressed with HA-tagged CK1ε WT or *tau* mutant in NIH 3T3 cells treated with CHX (40 μg/ml). Data shown are representative of at least three separate experiments.

modeling-based studies, later tested in cell-line studies (Gallego et al., 2006). Moreover, we show that this acceleration is a consequence of enhanced rates of degradation of PER proteins at specific phases of the circadian cycle i.e., early circadian night, and that such asymmetric effects on PER degradation are translated into altered phasing of physiological and behavioral circuits. Our studies also reveal that CK1ε^{*tau*} can act on both nuclear and cytoplasmic targets but suggest that within the SCN, CK1-mediated degradation may be primarily a nuclear event, as predicted by our studies of the hamster mutant (Dey et al., 2005). We also show that the knockout of Ck1ε has a relatively mild phenotype (extends the circadian period by ca 18 min a day) and that a single wild-type allele offer no significant protection in the presence of

the *tau* allele. A clear implication therefore is that CK1δ may phosphorylate target PERIOD proteins and that wild-type CK1ε may thus be partially redundant in the circadian timing mechanisms. Resolution of these issues awaits characterization of the phenotypes of *Ck1δ* knockouts.

An intriguing feature of our data is that the duration of molecular night is relatively compressed due to the accelerated clearance of PER2 after its peak expression at CT12, but the duration of nocturnal behavioral and physiological processes (CBT, melatonin secretion) is apparently normal, as measured in solar time. Consequently, because the offsets are not governed by the molecular cycle, they occur several hours later than the compressed molecular cycle would predict: nocturnal processes spilling over

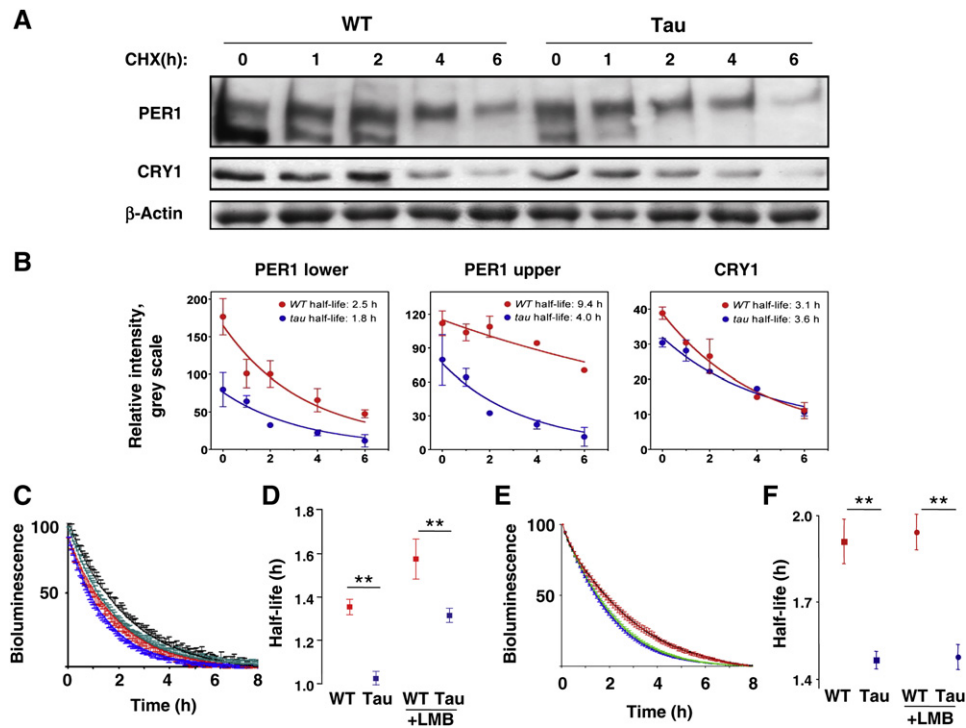


Figure 6. Degradation of Endogenous PER Is Accelerated in Tissue and Cells from *tau* Mutant Mice

(A) Representative western blots of endogenous PER1 and CRY1 in lung fibroblasts from WT or *tau* mice, treated with CHX (20 μ g/ml) for 0, 1, 2, 4, and 6 hr. Note two distinct bands for PER1.

(B) Group data (mean \pm SEM, red = WT, blue = mutant) from western blots reveal significant reduction in expression and earlier clearance of PER1 in mutant fibroblasts (F test, $p < 0.05$ for upper band) but no effect of *tau* on expression of endogenous CRY1 (F test, $p = 0.39$).

(C) Decay of PER2::LUC bioluminescence from lung fibroblasts, exposed to CHX in presence or absence of LMB. Data are normalized to the peak level of expression (time 0 after CHX) and the minimum after 8 hr and plotted as mean \pm SEM; red = WT + vehicle, black = WT + LMB, blue = *tau* + vehicle, green = *tau* + LMB).

(D) Half-lives for PER2::LUC bioluminescence from fibroblasts (mean \pm SEM). CK1 ϵ ^{*tau*} significantly accelerated loss of PER2::LUC signal regardless of LMB treatment. ** $p < 0.01$ by t test.

(E) Decay of PER2::LUC bioluminescence from SCN slices, exposed to CHX in the presence or absence of LMB. Data expressed as in (C).

(F) Half-lives for PER2::LUC bioluminescence from SCN slices (mean \pm SEM). CK1 ϵ ^{*tau*} significantly accelerated loss of PER2::LUC signal regardless of LMB treatment. ** $p < 0.01$ by t test.

into the start of the molecular day. Hence the behavioral day (defined by activity offset and onset) is shorter in the mutant, even though the underlying determining change is shortening of the molecular night. These strongly asymmetric effects of CK1 ϵ ^{*tau*} on molecular and behavioral timing likely underlie the pronounced disturbances of circadian timekeeping (damped amplitude, altered phasing) widely observed in the peripheral tissues of *tau* mutant hamsters (Dey et al., 2005) and may contribute to poor growth and general morbidity associated with the mutation in hamsters (Lucas et al., 2000). The variable responses of peripheral tissues to the *tau* mutation are intriguing and may suggest tissue-specific differences in the relative expression of CK1 ϵ or CK1 δ , or cellular differences in the manner in which PERIOD proteins are trafficked and degraded.

Endogenous PER (but not CRY) proteins (PER1 by western blot, PER2 by bioluminescence recording) are destabilized in the *tau* mutant background. These effects on protein half-life occur in a context (treatment with cycloheximide) where transcription is irrelevant and thus the observed protein instability is sufficient to explain the behavioral phenotype in full. This point is

reinforced by our original findings in the *tau* mutant hamster (Dey et al., 2005) which showed that the *Per* mRNA cycle in the SCN mapped to circadian time whereas the PER protein expression cycle was accelerated in vivo due to early clearance. These results from the kinase mutants therefore provide a valuable counterpoint to those of Xu et al. (2007), who modeled human FASPS by creating mice carrying transgenes encoding mutated versions of the human PER2 protein. The S662G mutation in *hPer2*, which leads to one form of FASPS in patients, shortened circadian period but the apparent degradation rate of PER2 protein was unaltered. Rather, expression of *hPer2* mRNA was reduced, leading to lower hPER2 protein levels. Our findings with the kinase mutant therefore add further support to the speculation of Xu et al. (2007) that effects mediated via S662 may accelerate the clock by reduced transcription, whereas the *tau* mutation, as a gain-of-function of CK1 ϵ , targets a separate domain within PER2 which is responsible for accelerated degradation.

The lack of impact of CK1 ϵ ^{*tau*} on CRY dynamics complements the recent description of loss-of-function mutations on F box

proteins, which mediate actions on CRY degradation, resulting in a longer half-life of CRY proteins (Godinho et al., 2007; Busino et al., 2007; Sieppka et al., 2007). As a result, circadian period is lengthened. These studies and data reported here further suggest that mechanisms for the degradation of these two core circadian transcription factor families (PER and CRY) operate independently but must have tightly coevolved in order to achieve precise overall control on circadian period. Our new mouse model therefore provides new insight into how a circadian mutation accelerates behavioral and cellular circadian rhythms, in both the brain and peripheral tissues, and demonstrates that temporally specific effects on PER degradation can be tracked through to an altered circadian structure of behavior and physiology.

EXPERIMENTAL PROCEDURES

Animal Maintenance

All experiments were conducted under the aegis of the 1986 Home Office Animal Procedures Act (UK) and following local ethical review. All animals were reared at 20°C–22°C and maintained on standard rodent breeder or maintenance chow under 12 hr light:12 hr dark lighting schedules.

Antibodies and Plasmids

Monoclonal anti-CK1 ϵ antibody was obtained from BD Transduction Laboratories, and anti-Myc (9E10) antibody from Santa Cruz Biotechnology. Anti-PER1 and Anti-CRY1 antibodies were a kind gift from Choogon Lee. Polyclonal anti-Myc antibody (9106) was from ABCAM and anti- α -Tubulin (T6199) and anti-actin (A2066) from Sigma. Myc-PER1 constructs were cloned in PCS2+MT vector and HA-tagged kinases (CK1 ϵ WT and *tau* mutant) were cloned in pCEP4 (Invitrogen). The SV40 Tag NLS (PKKKRKVG) was added to the 5' end of Myc-mPER1 by PCR (Gallego et al., 2006). Full-length mPer2 cDNA with C-terminal enhanced yellow fluorescent protein tag derived from pEYFP-N1 (Clontech) was cloned into pcDNA3.1/V5/HisA vector (Invitrogen) (PER2::YFP). Full-length mCry1 cDNA was cloned into enhanced cyan fluorescent protein vector pECFP-N1 (Clontech) (CRY1::CFP). *Tau* mutation plasmid for transfection was prepared by site directed mutagenesis leading to a substitution of arginine 178 (*C*GC) by cysteine (*T*GC). Kinase-dead variant was prepared by substitution of lysine at position 38 (AAG) by alanine (GCC). *Ck1 ϵ* plasmid was generously donated by Achim Kramer (Humboldt-university, Berlin, Germany). Wild-type, *tau*, or kinase-dead variants of full-length *Ck1 ϵ* cDNA were cloned into pcDNA-DEST40 vector (Invitrogen) (WT, Tau, KD).

Generation of Transgenic Mice

The targeting construct contained exons 2–6 of the *Ck1 ϵ* gene (Figure S1) was prepared using sv129 genomic DNA fragments from a PAC clone. Briefly, an 8.7 kb Sall–XbaI fragment encompassing exons 2–6 was subcloned into pBluescript (KS+) and verified by end-sequencing. The 1.4 kb BglII–EcoRI fragment containing exon 4 was used to introduce the *tau* mutation (C12555T) by site-directed mutagenesis and verified by sequencing. A floxed NeoTK selection cassette was inserted into the EcoRI site in the intron 4, and a double stranded oligo encoding lox P and NcoI sites ligated into the BglII site 5' of exon 4 (Figure S1A). The targeting construct was linearized with NotI, electroporated into 129/Sv R1 ES cells (<http://www.mshri.on.ca/nagy/r1.htm>), and genomic DNA from G418-resistant clones isolated as described previously (Talts et al., 1999). BglII-digested DNA was Southern blotted and hybridized with ³²P-labeled external probe, amplified from genomic DNA using the following primers: forward 5'-ACTTCCTTCTCTTTACCCACG-3'; reverse 5'-AGAAGCAAGCATCCATTTCC-3'. The floxed selection cassette was deleted from homologously recombined ES cell clones by transient transfection with a cre-expressing plasmid followed, 48 hr later, by 5 days of FIAU (1-(2-deoxy-2-fluoro- β -D-arabino-furanosyl)-5-iodouracil) selection (Abuin and Bradley, 1996). FIAU-resistant colonies were expanded and genomic DNA analyzed by PCR as described below to determine whether they were *tau* or knockout

alleles. ES cell clones carrying the *tau* allele (*tau*+) were used to create germline-transmitting chimeras by blastocyst injection. *tau*+/+ mice were crossed with littermates to produce homozygous *tau* offspring allele or crossed with a deleter cre line to generate the *Ck1 ϵ* knockout allele in vivo. Wild-type (+) and *tau* alleles were genotyped by PCR using primers "a" (5'-CACCTGGGCATTGGTGAGT-3') and "b" (5'-GGAGGTCAAGGGGCCAGT-3') (Figure S1A). The presence of the knockout (–) allele was detected using primers "c" (5'-GTGGTAGAAGGAGAGAACTGAC-3') and "b" (see above). In all, 11 chimeric mice derived from 3 clones were used to generate a founder line of *Ck1 ϵ* mice, which were then introgressed over six generations into a C57/B6 background.

RT-PCR

Total RNA from brain of CK1 ϵ knockout mice and wild-type siblings was isolated using Trizol (Invitrogen). To exclude genomic DNA contamination, total RNA was digested with DNase I (Roche). One microgram of total RNA was reverse transcribed using Oligo-dT oligonucleotides by the SuperScript II RNase H-Reverse Transcription kit (Invitrogen). In parallel, negative control samples lacked Reverse Transcriptase. Two microliters of the resultant first strand cDNA was PCR amplified with appropriate primer pairs using a hot-master PCR kit (Eppendorf) as follows: (1) 96°C for 5 min; (2) 30 \times 94°C for 20 s, 55°C for 10 s, 72°C for 50 s; (3) 72°C for 7 min. PCR products were visualized on 1.5% agarose gel. Primer pairs were based on mouse sequences as follows (all 5'–3'): *Ck1 ϵ* forward, GCCTCTGGTGAGGAAGTAG; reverse, CGGTAGGGAATATGCTGGTG. *Gapdh* forward, CCTTCATTGACCTCAACTAC; reverse, GGAAGCCATGCCAGTGAGC.

Western Blotting of CK1 ϵ

Protein extracts were prepared from whole brain of wild-type, CK1 ϵ knockout, and CK1 ϵ ^{*tau/tau*} mice. Mice were euthanized by cervical dislocation; whole brains were removed and frozen on dry ice. Tissues were mechanically homogenized at 4°C in three volumes of extraction buffer (0.1 M KCl, 20 mM HEPES [pH 7.5], 5 mM EDTA, 1 mM dithiothreitol, 0.1% Triton X-100, 5% glycerol, 0.5 mM phenylmethylsulfonyl fluoride [PMSF], 1 mM MgCl₂, 10 μ g/ml of aprotinin, 5 μ g/ml of leupeptin, 1 μ g/ml of pepstatin A). Homogenates were cleared by centrifugation (2 \times 10 min, 13,000 \times g at 4°C). Supernatants were mixed with 2 \times protein loading buffer, boiled, and spun at 13,000 \times g for 1 min at room temperature. Total protein (70 μ g) was resolved on 10% denaturing PAGE gels and transferred to nitrocellulose membrane (Bio-Rad). Membranes were blocked with 5% skimmed milk in Tris-buffered saline containing 0.05% Tween 20 and incubated with relevant antibodies. ECL plus detection was used (Amersham Biosciences).

Behavioral Analysis

Six- to sixteen-week-old mice were single-housed in cages equipped with running wheels and ad libitum food and water, contained within a light-tight chamber at constant temperature (°C) and humidity (% H₂O). Mice were entrained to a 12hr light and 12 hr dark (LD) cycle for 7 days and released into constant darkness (DD) for ~28 days. Wheel revolutions were recorded in 10 min time bins by DataQuest III acquisition program (Data Sciences Inc.), transferred to the TauActo 1.2 analysis software (developed in house by T. Brown) to produce double-plotted actograms, periodogram, intensity of running (alpha/rho), and power of rhythm. χ^2 periodogram analyses were performed using 28 days of data in DD.

Electrophysiological Recordings

Electrophysiological recordings were conducted and analyzed as previously described (Brown et al., 2006). Mice (housed with running wheels in DD) were killed at the beginning of the inactive phase, and coronal brain sections (350 μ m thick) were cut using a vibroslicer (Campden Instruments) and transferred to an interface style brain slice chamber continuously perfused (~1.5 ml/min) with oxygenated (95% O₂/5% CO₂) aCSF supplemented with 0.0005% gentamicin (Sigma) and warmed to 36°C \pm 1°C. Extracellular multi-unit activity (MUA, signal-to-noise > 2:1) was recorded from the SCN using aCSF-filled suction electrodes, differentially amplified (\times 20,000) and band-pass filtered (300–3000 Hz) via a Neurolog system (Digitimer), digitized (25,000 Hz) using a micro 1401 mkII interface (Cambridge Electronic Design [CED]), and recorded on a PC running Spike2 version 5 software (CED).

Single-unit activity was discriminated from MUA recordings offline on the basis of waveform shape and validated by measurement-based clustering and the presence of a clear refractory period in an interspike interval histogram. Firing rate data were moderately smoothed using a 1 hr moving average and presented as the mean firing rate each min. The circadian period of single-cell and MUA rhythms were analyzed by curve-fitting developed in-house (Clockwise; Dr. T. Brown). Initially, data were normalized such that data spanned a range of values between 100 and -100 . The normalized data were then fit with the equation $Y = A \sin(B(x+C))$ using the Newton-Raphson iterative method, where A equaled the amplitude of the rhythm, B equaled the period in radians/hr and C determined the phase. Initial values of A, B, and C were estimated from the best fitting curve of a series of >3000 standard curves that spanned the period range 3–34 hr and exhibited a range of different amplitudes and phasing. Peak widths were defined as the duration over which firing rate was above the mean for that cell.

Metabolic Rhythm Measurement and Analysis

Indirect Calorimetry

Tau and WT mice ($n = 6$ per genotype) were single-housed in indirect calorimetric cages (Columbus Instruments). Mice were monitored for a minimum of 10 days in LD followed by a minimum of 5 days in constant light (LL), during which time oxygen consumption (VO_2) was measured every 10 min. Illustrations of VO_2 traces in Figure 2 depict group (genotype) averages taken from a representative experiment.

Analysis of Metabolic Rhythms

Circadian rhythms in VO_2 were analyzed using curve-fitting software (Clockwise) as described above. Recordings from individual animals during LD and LL portions of the experiment were analyzed separately. Once period length was determined, a composite circadian cycle of metabolic rate was generated for each animal from the entire test period (a separate composite was generated for each lighting condition). From these representative circadian profiles, “active” and “inactive” portions of the cycle were determined by normalizing metabolic rate to the midpoint (50%) of the peak to trough amplitude, calculated separately for the rise and fall of the rhythm. Duration of active and inactive phases in LD and LL was analyzed using repeated-measures two-way ANOVA, with a Bonferroni's post hoc test.

Bioluminescence Recording and Imaging

Whole-slice bioluminescence emission and individual cellular emission were recorded as described (Maywood et al., 2006; Prosser et al., 2007) using photomultiplier assemblies and CCD cameras supplied by Hamamatsu. Waveforms of rhythmic bioluminescence emission from whole slices and individual cells were analyzed in BRASS software and RAP algorithm.

Cell Isolation, Culture, and Transfection

For culture of primary lung fibroblast, lungs were removed from euthanized adult mice for peripheral fibroblast preparation. Briefly, lung was chopped and minced in sterile conditions and washed twice in chilled modified Hank's Balanced Salt Solution (Sigma). Cells were then dissociated by means of shaking at 37°C for 2 hr in 100 u/ml of Collagenase IA (Sigma) (dissolved in PBS) and 3 mM $CaCl_2$. Once dissociated, cells were filtered through a sterile nylon mesh followed by two washes and centrifugation in chilled Hank's solution. Pellets were resuspended in culture medium (DMEM with 4.5 g/l glucose, Glutamax, and pyruvate, supplemented with 10% FBS, 100 U/ml Penicillin, and 100 μ g/ml streptomycin) and plated on a 10 cm culture dish. Cultures were maintained at 37°C (5% CO_2) for 2–3 days until confluent and ready for splitting. Confluent cells in 35 mm dishes were synchronized with Dexamethasone (100 nM) for 1 hr prior to PMT recording of PER2::LUC bioluminescence (Izumo et al., 2003).

NIH 3T3 cells were grown in DMEM supplemented with 10% calf serum and antibiotics. At 90% confluence in 6-well plates, cells were transfected with relevant plasmid combinations using Lipofectamine 2000 (Invitrogen). The amount of transfected DNA was 0.8 μ g of *Myc-Per1* and 0.4 μ g encoding HA-tagged kinases for each well. COS-7 cells were grown in DMEM supplemented with 10% calf serum and antibiotics. At 80%–90% confluence in glass-bottomed dishes (MatTek), cells were transfected with combinations of relevant plasmids using 3 μ l of GeneJuice (Novagen). The total amount of transfected DNA was 1 μ g (0.6 μ g of *Per2::YFP* + 0.4 μ g of CK1 ϵ or 0.5 μ g

of *Cry1::CFP* + 0.5 μ g of CK1 ϵ) for each dish. Twenty-four hours after transfection, DMEM was exchanged for air medium and subjected to live cell fluorescent imaging (Maywood et al., 2006).

Protein Degradation Assay

For real-time monitoring of PER2::YFP and CRY1::CFP degradation, COS-7 cells were treated with 20 μ g/ml cycloheximide (Sigma), with or without LMB pretreatment (10 ng/ml for 1 hr; Calbiochem). Fluorescence was recorded every 15 min for at least 17 hr by time-lapse microscopy using Openlab software (Improvision, Warwick, UK). Single cell fluorescent data were analyzed by IPlab software (Scanalytics, B.D. Bioscience, Rockville, MD) and one-phase exponential decay curve fitting. Half-life calculations and statistics were performed in Prism (GraphPad Software). Data were plotted as mean \pm SEM with fitted exponential decay curve. Half-lives are plotted as mean \pm 95% confidence interval of exponential decay curve fitting.

For detection of Myc-tagged PER1 degradation by western blotting, 20 hr after transfection, cells were treated with CHX (40 μ g/ml) for 0, 2, and 4 hr and then lysed in lysis buffer (150 mM NaCl/20 mM HEPES [pH 7.5]/0.1% Nonidet P-40/1 mM EDTA/2 mM DTT) supplemented with 1 \times Complete protease inhibitor mixture (Roche Applied Science). The cells were then mechanically sheared, and lysates were centrifuged at 16,000 \times g for 10 min at 4°C. Total protein (100 μ g) was resolved in SDS/PAGE and then subject to western blotting. For endogenous PER1 and CRY1 degradation, primary lung fibroblasts were treated with CHX (20 μ g/ml) for 0, 1, 2, 4, and 6 hr then subjected to western blotting using anti-PER1 and anti-CRY1 antibodies. These experiments were duplicated. For real-time monitoring of PER2::LUC degradation by PMT, SCN slices or lung fibroblasts were treated with CHX (40 μ g/ml) with or without LMB pretreatment (10 ng/ml for 1 hr). For control experiments, DMSO (for CHX) or ethanol (for LMB) was used as vehicle.

Immunostaining of PER1 and Mutants in NIH 3T3 Cells

Twenty hours after transfection of different PER1 constructs, cells were replated on glass coverslips. Twenty-four hours later, cells were washed three times with phosphate-buffered saline (PBS) and fixed with 3.7% paraformaldehyde for 15 min. After three more washes, cells were permeabilized with 0.1% Triton X-100 in PBS for 5 min and washed with 3% BSA/0.1% TX-100/PBS for 30 min. Cells were incubated with an anti-Myc polyclonal antibody for 1 hr in 3% BSA/0.1% TX-100/PBS, washed three times, and incubated with a secondary Alexa Fluor 594 goat anti-rabbit IgG (Molecular Probes, Inc.) for 1 hr. Cells were washed three and incubated with DAPI (1 μ g/ml) in 0.1% TX-100/PBS. Cells were visualized using an Olympus AX70 fluorescence microscope (magnification \times 60), and images were digitally recorded via an AxioCam (Carl Zeiss Microimaging, Inc.) and saved using the AxioVision 3.1 program. Overlays of the immunofluorescence images were performed in Photoshop (Adobe).

SUPPLEMENTAL DATA

The Supplemental Data for this article can be found online at <http://www.neuron.org/cgi/content/full/58/1/78/DC1/>.

ACKNOWLEDGMENTS

We thank Tracey Butcher, Graham Morrissey, Emma Owens, Sarah Atkinson, Helen Lydon, Jian Li, Julie Gibbs, and Shin Yamazaki for technical assistance. We thank Russell Foster, Owen Jones, and Rob Lucas for comments on the manuscript, Simon Luckman for access to the metabolic monitoring equipment (CLAMS), and Andrew Millar for BRASS software package, Masahiro Ishiura for RAP software package. We thank A. Kramer for kind provision of research materials. The project was supported by the Biotechnology and Biological Sciences Research Council and Medical Research Council of the UK for funding.

Received: October 22, 2007

Revised: December 17, 2007

Accepted: January 24, 2008

Published: April 9, 2008

REFERENCES

- Abuin, A., and Bradley, A. (1996). Recycling selectable markers in mouse embryonic stem cells. *Mol. Cell. Biol.* **16**, 1851–1856.
- Brown, T.M., Hughes, A.T., and Piggins, H.D. (2005). Gastrin-releasing peptide promotes suprachiasmatic nuclei cellular rhythmicity in the absence of vasoactive intestinal polypeptide-VPAC2 receptor signaling. *J. Neurosci.* **25**, 11155–11164.
- Brown, T.M., Banks, J.R., and Piggins, H.D. (2006). A novel suction electrode recording technique for monitoring circadian rhythms in single and multiunit discharge from brain slices. *J. Neurosci. Methods* **156**, 173–181.
- Busino, L., Bassermann, F., Maiolica, A., Lee, C., Nolan, P.M., Godinho, S.I., Draetta, G.F., and Pagano, M. (2007). SCFFbx3 controls the oscillation of the circadian clock by directing the degradation of cryptochrome proteins. *Science* **316**, 900–904.
- Dey, J., Carr, A.J., Cagampang, F.R., Semikhodskii, A.S., Loudon, A.S., Hastings, M.H., and Maywood, E.S. (2005). The tau mutation in the Syrian hamster differentially reprograms the circadian clock in the SCN and peripheral tissues. *J. Biol. Rhythms* **20**, 99–110.
- Eide, E.J., Vielhaber, E.L., Hinz, W.A., and Virshup, D.M. (2002). The circadian regulatory proteins BMAL1 and cryptochromes are substrates of casein kinase I ϵ . *J. Biol. Chem.* **277**, 17248–17254.
- Gallego, M., and Virshup, D.M. (2007). Post-translational modifications regulate the ticking of the circadian clock. *Nat. Rev. Mol. Cell Biol.* **8**, 139–148.
- Gallego, M., Eide, E.J., Woolf, M.F., Virshup, D.M., and Forger, D.B. (2006). An opposite role for tau in circadian rhythms revealed by mathematical modeling. *Proc. Natl. Acad. Sci. USA* **103**, 10618–10623.
- Godinho, S.I., Maywood, E.S., Shaw, L., Tucci, V., Barnard, A.R., Busino, L., Pagano, M., Kendall, R., Quwallid, M.M., Romero, M.R., et al. (2007). The after-hours mutant reveals a role for Fbx3 in determining mammalian circadian period. *Science* **316**, 897–900.
- Hastings, M.H., Reddy, A.B., and Maywood, E.S. (2003). A clockwork web: circadian timing in brain and periphery, in health and disease. *Nat. Rev. Neurosci.* **4**, 649–661.
- Izumo, M., Johnson, C.H., and Yamazaki, S. (2003). Circadian gene expression in mammalian fibroblasts revealed by real-time luminescence reporting: Temperature compensation and damping. *Proc. Natl. Acad. Sci. USA* **100**, 16089–16094.
- Kloss, B., Price, J.L., Saez, L., Blau, J., Rothenfluh, A., Wesley, C.S., and Young, M.W. (1998). The *Drosophila* clock gene *double-time* encodes a protein closely related to human casein kinase 1 ϵ . *Cell* **94**, 97–107.
- Lee, C., Etchegaray, J.P., Cagampang, F.R., Loudon, A.S., and Reppert, S.M. (2001). Posttranslational mechanisms regulate the mammalian circadian clock. *Cell* **107**, 855–867.
- Lowrey, P.L., and Takahashi, J.S. (2004). Mammalian circadian biology: elucidating genome-wide levels of temporal organization. *Annu. Rev. Genomics Hum. Genet.* **5**, 407–441.
- Lowrey, P.L., Shimomura, K., Antoch, M.P., Yamazaki, S., Zemenides, P.D., Ralph, M.R., Menaker, M., and Takahashi, J.S. (2000). Positional syntenic cloning and functional characterization of the mammalian circadian mutation tau. *Science* **288**, 483–492.
- Lucas, R.J., Stirling, J.A., Darrow, J.M., Menaker, M., and Loudon, A.S. (1999). Free running circadian rhythms of melatonin, luteinizing hormone, and cortisol in Syrian hamsters bearing the circadian tau mutation. *Endocrinology* **140**, 758–764.
- Lucas, R.J., Stirling, J.A., Mohammad, Y.N., and Loudon, A.S. (2000). Postnatal growth rate and gonadal development in circadian tau mutant hamsters reared in constant dim red light. *J. Reprod. Fertil.* **118**, 327–330.
- Maywood, E.S., Reddy, A.B., Wong, G.K.Y., O'Neil, J., O'Brien, J.A., McMahon, D.G., Harmar, A.J., and Hastings, M.H. (2006). Synchronization and maintenance of timekeeping in superchiasmatic circadian clock cells by neuropeptidergic signalling. *Curr. Biol.* **16**, 599–605.
- Mignot, E., and Takahashi, J.S. (2007). A circadian sleep disorder reveals a complex clock. *Cell* **128**, 22–23.
- Price, J.L., Blau, J., Rothenfluh, A., Abodeely, M., Kloss, B., and Young, M.W. (1998). *double-time* is a novel *Drosophila* clock gene that regulates PERIOD protein accumulation. *Cell* **94**, 83–95.
- Prosser, H.M., Bradley, A., Chesham, J.E., Ebling, F.J.P., Hastings, M.H., and Maywood, E.S. (2007). Prokineticin receptor 2 (*Prokr2*) is essential for the regulation of circadian behavior by the suprachiasmatic nuclei. *Proc. Natl. Acad. Sci. USA* **104**, 648–653.
- Ralph, M.R., and Menaker, M. (1988). A mutation of the circadian system in golden hamsters. *Science* **241**, 1225–1227.
- Reppert, S.M., and Weaver, D.R. (2002). Coordination of circadian timing in mammals. *Nature* **418**, 935–941.
- Saper, C.B., Scammell, T.E., and Lu, J. (2005). Hypothalamic regulation of sleep and circadian rhythms. *Nature* **437**, 1257–1263.
- Siepkka, S.M., Yoo, S.H., Park, J., Song, W., Kumar, V., Hu, Y., Lee, C., and Takahashi, J.S. (2007). Circadian mutant overtime reveals F-box protein FBXL3 regulation of cryptochrome and period gene expression. *Cell* **129**, 1011–1023.
- Talts, J.F., Brakebusch, C., and Fassler, R. (1999). Integrin gene targeting. *Methods Mol. Biol.* **129**, 153–187.
- Toh, K.L., Jones, C.R., He, Y., Eide, E.J., Hinz, W.A., Virshup, D.M., Ptacek, L.J., and Fu, Y.H. (2001). An hPer2 phosphorylation site mutation in familial advanced sleep phase syndrome. *Science* **291**, 1040–1043.
- Vanselow, K., Vanselow, J.T., Westermark, P.O., Reischl, S., Maier, B., Korte, T., Herrmann, A., Herzog, H., Schlosser, A., and Kramer, A. (2006). Differential effects of PER2 phosphorylation: molecular basis for the human familial advanced sleep phase syndrome (FASPS). *Genes Dev.* **20**, 2660–2672.
- Vielhaber, E.L., Duricka, D., Ullman, K.S., and Virshup, D.M. (2001). Nuclear export of mammalian PERIOD proteins. *J. Biol. Chem.* **276**, 45921–45927.
- Xu, Y., Padiath, Q.S., Shapiro, R.E., Jones, C.R., Wu, S.C., Saigoh, N., Saigoh, K., Ptacek, L.J., and Fu, Y.H. (2005). Functional consequences of a CK1 δ mutation causing familial advanced sleep phase syndrome. *Nature* **434**, 640–644.
- Xu, Y., Toh, K.L., Jones, C.R., Shin, J.Y., Fu, Y.H., and Ptacek, L.J. (2007). Modeling of a human circadian mutation yields insights into clock regulation by PER2. *Cell* **128**, 59–70.
- Yoo, S.H., Yamazaki, S., Lowrey, P.L., Shimomura, K., Ko, C.H., Buhr, E.D., Siepkka, S.M., Hong, H.K., Oh, W.J., Yoo, O.J., et al. (2004). PERIOD2:LUCIFERASE real-time reporting of circadian dynamics reveals persistent circadian oscillations in mouse peripheral tissues. *Proc. Natl. Acad. Sci. USA* **101**, 5339–5346.